JMEPEG (2009) 18:538–542
DOI: 10.1007/s11665-009-9494-7

1059-9495/$19.00

Surface Form Memory in NiTi: Energy Density of Constrained Recovery During Indent Replication

Xueling Fei, Corey J. O'Connell, David S. Grummon, and Yang-Tse Cheng

(Submitted October 7, 2008; in revised form February 9, 2009)

Spherical indentation of NiTi shape memory alloys (SMA) to depths greater than about 3% of the indenter radius results in two-way shape-memory training in a deformation zone beneath the indent. If deep spherical or cylindrical indents are subsequently machined away just sufficiently to remove traces of the original indent (in the martensitic condition), a thermally induced and cyclically reversible flat-to-protruded surface topography is enabled. We term the phenomenon surface form memory. The amplitude of cyclic protrusions, or 'exdents', is related to the existence of a subsurface deformation zone in which indentation has resulted in plastic strains beyond that which can be accomplished by martensite detwinning reactions. Dislocation generation in this zone is thought to underlie the observed two-way shape-memory (TWSME) training effect. In this article, we show that these cyclic exdents can perform appreciable mechanical work when displacing under load against a base-metal substrate (constrained recovery). This "non-Hertzian" indentation, which appears to be able to exert the full energy density of SMA actuation, may have use for assembly of micromachines, bond-release, microforging, microjoining, electrical switching, microconnectors, and variable heat transfer devices, among many other potential applications.

Keywords energy density, NiTi, shape memory, surfaces

1. Introduction

Several groups have investigated shape memory and superelastic effects using micro- and nanoindentation techniques (Ref 1-5). Recently, Zhang et al. (Ref 6, 7) reported thermally reversible flat-to-bumpy surface transitions using an indentation-planarization method applied to both wrought and thin film NiTi. The planarization step, which removes visible traces of the indent, converts an indented surface having two-way indent depth change to one with thermally controllable *form*.

The essential features of the technique are schematically illustrated in Fig. 1. Here, r is the initial indenter radius, a is the indent contact radius, and h is the initial indent depth. The ratio a/r can be used to characterize the representative strain, ε_r, produced by the indent, which in turn correlates with the plastic component of total strain in tensile tests (Ref 8, 9). For spherical indenters, $\varepsilon_r = 0.2\ a/r$. Previous work has shown that two-way indent recovery effects are observed only when a/r exceeds 0.25, equivalent to $\varepsilon_r = 0.05$, i.e., the strain corresponding to the end of the detwinning plateau in tensile deformation of martensitic NiTi.

Both the amplitude of reversible indent depth changes (δ_1 in Fig. 1) and the height δ_2 of the surface protrusions (exdents) can be related to the depth of a subsurface zone in which indentation has induced strains beyond those that can be mediated by deformation twinning reactions in the martensite. Dislocation production in this zone probably accounts for the observed two-way effect. The depth, D^*, of this 'active' zone has been determined by experiment (as described elsewhere, Ref 10) for both spherical and cylindrical indentation. As can be seen in Fig. 2, which plots the exdent height, δ_2, as a function of measured values of D^*, indicates that an average reversible strain within the active zone of ~2.4% can account for the observed displacements.

For surface form memory (SFM) to be useful as an actuation strategy, or for application to variable-friction surfaces, mold-release, or lithographic devices, it is necessary to demonstrate that useful work can be extracted during austenitization, i.e., that SFM can operate robustly in a constrained-recovery mode.

In this article, we present results on experiments designed to estimate the mechanical work that can be exerted by spherical protrusions when they displace against a base-metal substrate, and thereby produce a 'replicant' indent. It is shown that, by conservative estimate, the energy density associated with constrained recovery in SFM is on the order of the maximum generally available from NiTi actuators.

2. Experiments

A 3 mm thick 50.26 at.% Ni wrought NiTi alloy sheet acquired from Special Metals Corporation had transformation temperatures, M_f, M_s, A_s, and A_f, of 22, 58, 70, and 110 °C

This article is an invited paper selected from presentations at Shape Memory and Superelastic Technologies 2008, held September 21-25, 2008, in Stresa, Italy, and has been expanded from the original presentation.

Xueling Fei, Corey J. O'Connell, and **David S. Grummon**, Department of Chemical Engineering and Materials Science, Michigan State University, East Lansing, MI 48824; and **Yang-Tse Cheng**, Department of Chemical and Materials Engineering, University of Kentucky, Lexington, KY 40506. Contact e-mail: grummon@egr.msu.edu.

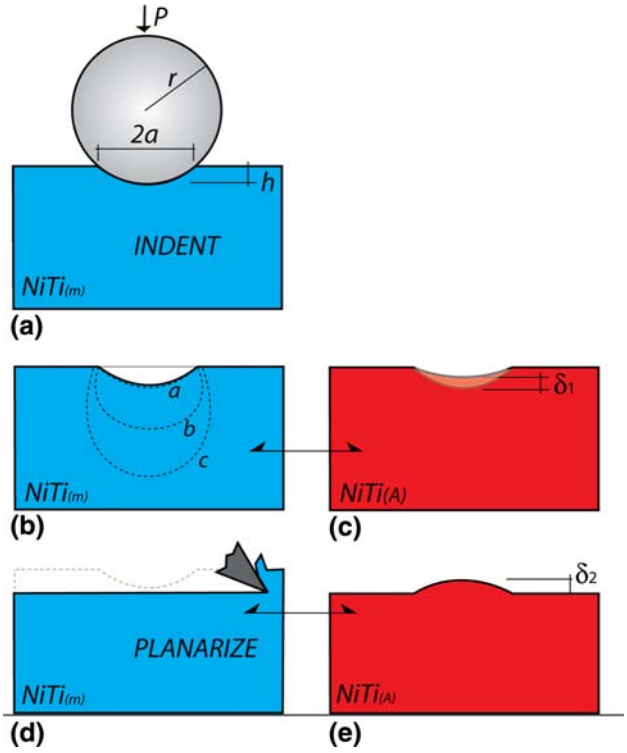

Fig. 1 Indent training (a-c) and planarization (d) to obtain surface form memory (SFM) 'exdents' in NiTi. Thermally cycling between (b) ↔ (c) and (d) ↔ (e) is indefinitely repeatable

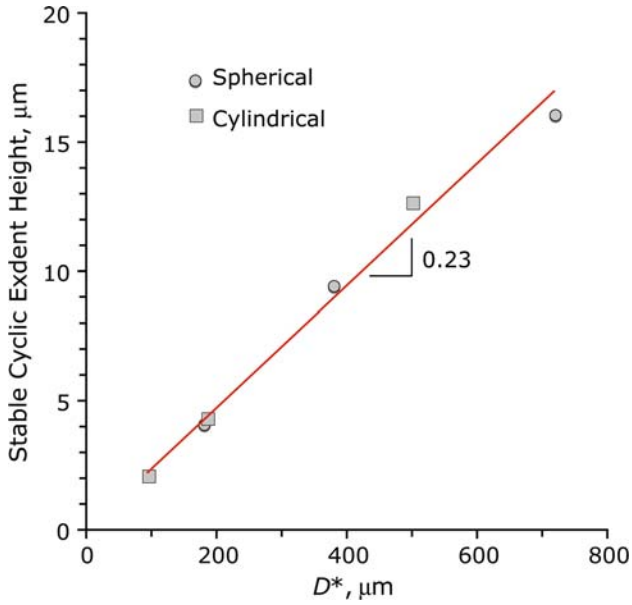

Fig. 2 Stable cyclic protrusion height for spherical and cylindrical indents as a function of the depth of the subsurface active zone, D^*. The slope of the linear curve fit gives an average strain in the volume defined by D^* of ~2.4%

respectively, as determined by differential scanning calorimetry. Specimens were first electrodischarge cut into 12.7 mm diameter discs and manually ground with 2000-grit SiC paper. They were then machine polished at room temperature with 0.05 μm colloidal silica. Before indentation, the specimens were chilled to approximately −50 °C to ensure a fully martensitic condition before later indentation at room temperature.

Table 1 Initial spherical indents into martensitic NiTi

Load, N	Depth, μm	Contact radius (*a*), μm	*a/r* ratio
200	37	167	0.42
700	107	271	0.68
3000	380	397	1.00

Spherical indents were made with an 0.794 mm diameter tungsten carbide ball using loads of 200, 700, and 3000 N. Each sample was indented at the same location twice since this had been found in previous work to give a stronger training effect. Surface profiles of the as-indented surfaces were acquired with a WYKO NT 1000 optical surface profilometer. The loads used gave *a/r* ratios of 0.42, 0.68, and 1.0, respectively, as summarized in Table 1. After indentation, and while still in the martensitic condition, the surfaces were ground and polished just enough to remove visible traces of the indent.

Constrained-recovery experiments were designed to obtain a rough estimate of the work output of the protrusions during constrained recovery. After planarization, the optically flat NiTi samples were placed in contact with coupons of 3 mm thick 6061-T6 aluminum and positioned between compression platens in a screw-driven load frame. The NiTi-aluminum sandwich was preloaded to a compressive stress of 100 MPa to insure positive contact. The assembly was then slowly heated by convection to 150 °C to austenize the NiTi, thus allowing the NiTi exdent to indent the aluminum coupon. (Thermal expansion in the assembly caused the stress to rise to about three times the initial preload.) Dimensional profiles of the indented aluminum surfaces were subsequently acquired using the WYKO profilometer. Additionally, profiles were obtained for the residual exdents in the NiTi samples, both directly following the indent replication experiment (at room temperature), and also in the austenitic condition, with samples heated to 150 °C, in situ in the profilometer stage, using a thermoelectric module.

To provide a basis for estimation of the work output of the NiTi exdent, conventional spherical indents were made in the same 6061-T6 aluminum plate using a 6.3 mm diameter tungsten ball under various loads. The diameter of this ball was chosen to match the radius of curvature of the replicant indents. Indents that were found to have *a/r* ratios comparable to those of the replicants were chosen to provide force-displacement data to give a rough measure of the work of conventional (Hertzian) indentation in 6061-T6 aluminum.

3. Results and Discussion

3.1 Spherical Replicant Indents in Aluminum

Surface profiles of replicant indents are shown in Fig. 3, together with profiles of the corresponding NiTi exdents taken at room temperature after the replicants were made. Measurements derived from these profiles are summarized in Table 2, which additionally includes measurement of the austenitic

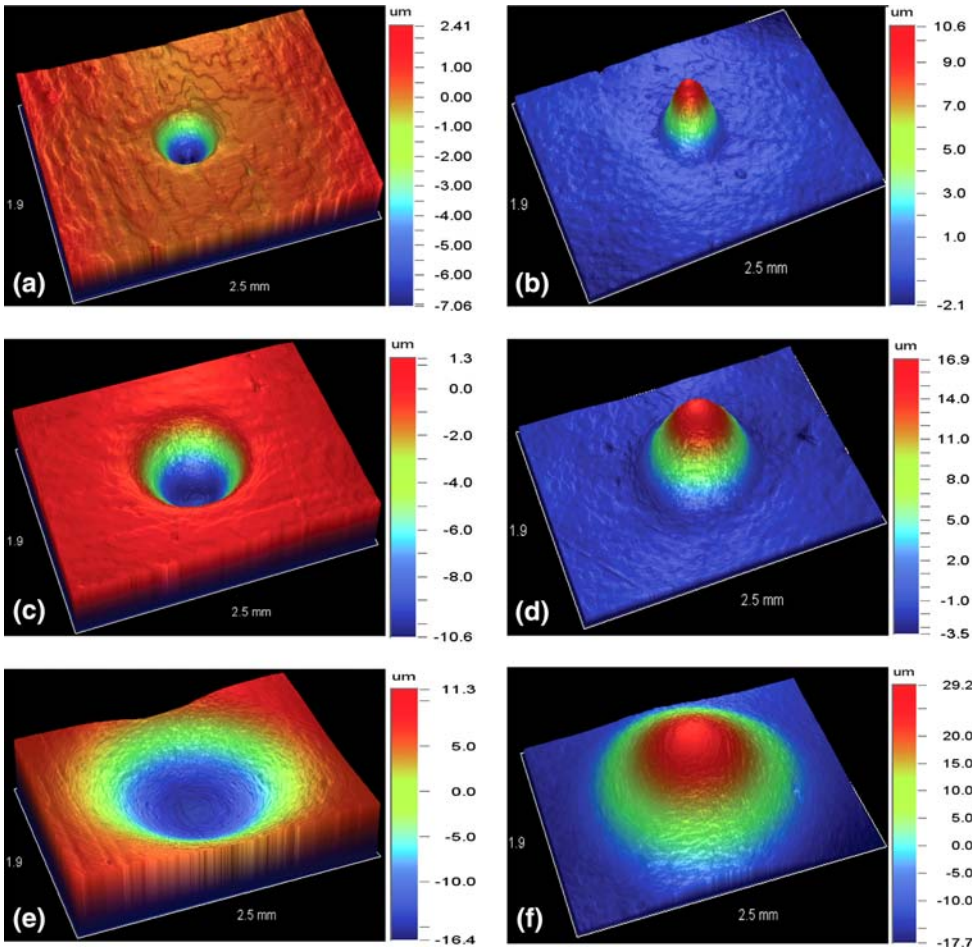

Fig. 3 Replicant indents in aluminum (left) and residual exdents in NiTi at 20 °C made directly following the replication experiment. Images (a, b), (c, d) and (e, f) correspond to initial indent *a/r* ratios of 0.42, 0.68, and 1.00, respectively. In each image, the field size is 1.9 mm × 2.5 mm. Vertical scales vary, as shown

Table 2 Replicant indent and residual exdent dimensions

Initial indent *a/r* ratio	Replicant indent depth (d_{repl}), µm	Replicant radius of curvature, µm	Replicant indent *a/r* ratio	NiTi exdent height, µm	
				20 °C	150 °C
0.42	7.1	3,808	0.061	10.7	16.4
0.68	11.4	8,812	0.051	20	27.6
1.00	25.8	15,443	0.058	42	51.2

exdent height after the replication experiment with NiTi samples re-heated to 150 °C in the profilometer. The latter measurement may be construed as the free-recovery amplitude of the exdents.

The replicant indent depth (normalized to the original indenter radius) is plotted as a function of the initial indentation *a/r* ratio in Fig. 4. The curve-fit shown is a second-order polynomial (constrained to pass through the origin) which achieved an R^2 value of 0.977. From this it may be concluded that, for the maximum initial indent *a/r* ratio of 1.0 (i.e., indentation of NiTi to a depth equal to the indenter radius), a

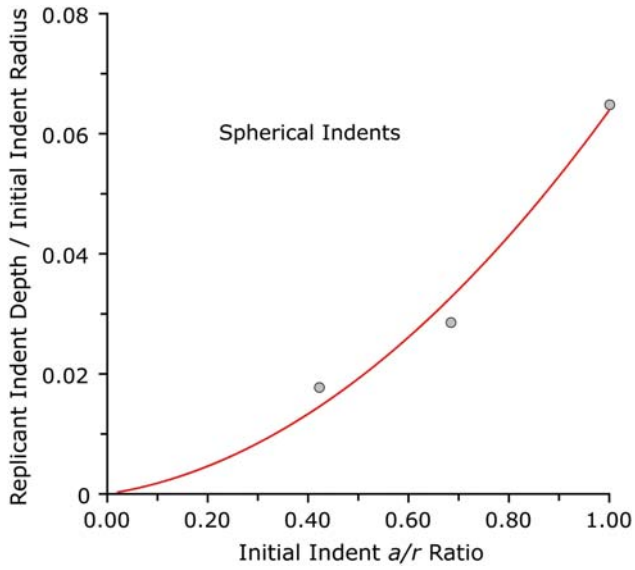

Fig. 4 Depth of replicant indents (normalized to the initial NiTi indenter radius) plotted as a function of the initial indent *a/r* ratio

replicant indent can be produced in 6061-T6 aluminum that has a depth that is approximately 6.5% of the initial NiTi indenter radius. This value declines to less than 2% for an initial *a/r* ratio of 0.42.

It is also of interest to compare the replicant indent depth to the height of the corresponding NiTi exdent in the austenitic condition at 150 °C (see leftmost column in Table 2). This is shown in Fig. 5 which plots these measurements, together with results of similar experiments conducted using cylindrical indenters to be described in detail elsewhere. For the present case of indent replication in 6061-T6 aluminum, a simple relationship between these two quantities emerges: The replicant indent depth, for both spherical and cylindrical indentation, is approximately half (47%) of the austenitic exdent height. The difference may be presumed to be composed of elastic springback in the aluminum and limitation of the SFM displacement under the imposed constraint conditions.

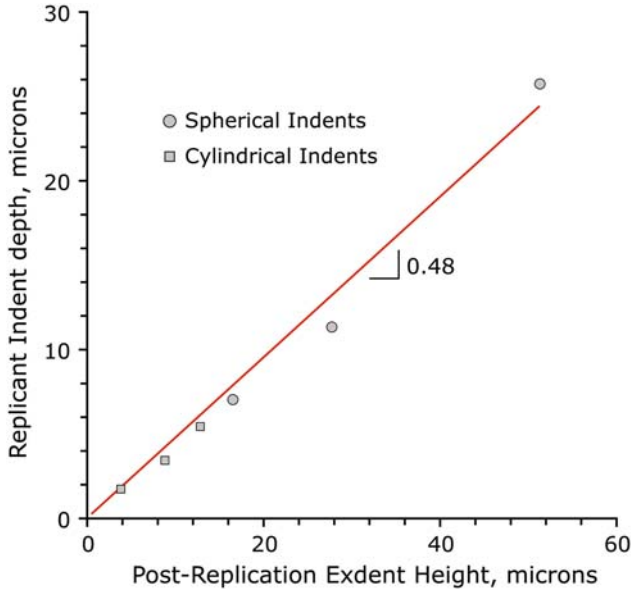

Fig. 5 The depth of replicant indents plotted as a function of the postreplication height of corresponding NiTi exdents when re-warmed to 150 °C (austenitic condition)

Experiments are under way on various different replication-substrate alloys to further study these relationships.

3.2 Calibration Indents in Aluminum

We have made a very rough approximation of the apparent energy density associated with exdent formation during constrained recovery in SFM. This has been accomplished by making conventional spherical indents in 6061-T6 aluminum using a ball with a radius close to that found for replicant indents in the study, and indenting to *a/r* ratios that are also close to those for of the replicants. Results for these calibration indentations are given in Table 3. For *a/r* ratios between 0.51 and 0.68, these experiments determined the spherical indentation hardness (H_{Al}, defined as the load divided by the projected contact area) to be ~1.3 GPa.

The projected contact area during replicant indentation is then calculated as $A_{repl} = \pi a_{repl}^2$ allowing us to estimate the peak replication force (assumed to be an increment above the preload force) as $P_{repl} = A_{repl} H_{Al}$. The energy of indentation then becomes $U_i = 1/2 P_{repl} d_{repl}$.

To obtain the effective energy density, it is necessary to make an estimate of the volume of material in which shape-memory recovery occurs, i.e., the active subsurface volume contributing to formation of the exdent. Previous experiments to determine the active volume that drives exdent formation (producing the results shown in Fig. 2) were made on specimens which had been planarized after having been thermally cycled several times between M_f and A_f, such that exdent formation was cyclically stable. In these cases, only the two-way component of shape memory is retained, and the depth of the active zone, D^*, was found to be on the order of 1.5 times the contact radius for the initial indent. (This is a depth that can be well correlated with the 5 to 7% strain contour in the subsurface deformation zone.)

However, in the present case, exdent formation without prior thermal cycling occurs by one-shot shape memory, and the depth of the active zone should extend roughly to the elastic-plastic boundary for the initial indent. This depth is not known directly in the present case, but experimental work on conventional spherical indentation in work-hardening materials (Ref 11) suggests that it is on the order of four times the contact radius. To arrive at a conservative estimate, we have adopted the latter approximation for D^*.

Table 3 Calibration indentation data for 6061-T6 aluminum

Indent depth, μm	Load, N	Indenter radius, m	*a/r* ratio	Contact radius, m	Contact area, m^2	Hardness (H_{Al}), Pa
4	100	3.08E − 03	0.051	1.57E − 04	7.75E − 08	1.29E + 09
5.2	135	3.08E − 03	0.058	1.79E − 04	1.00E − 07	1.35E + 09
5.7	150	3.08E − 03	0.061	1.88E − 04	1.11E − 07	1.35E + 09

Table 4 Quantities used in the calculation of energy density

Indent depth in Al, μm	Replicant contact radius (a_{repl}), μm	Replicant *a/r* ratio	Replicant contact area (A_{repl}), m^2	Equivalent replicant load (P_{repl}), N	Indentation energy (U), J	Estimated D^*, m	Estimated active volume (V^*), m^3	Estimated energy density, J/m^3
7.1	232.29	0.061	1.70E − 07	2.19E + 02	7.76E − 04	6.68E − 04	6.24292E − 10	1.24E + 06
11.4	449.41	0.051	6.35E − 07	8.54E + 02	4.87E − 03	1.08E − 03	2.66776E − 09	1.83E + 06
25.8	895.69	0.058	2.52E − 06	3.41E + 03	4.40E − 02	1.59E − 03	8.36174E − 09	5.26E + 06

With the further simplifying assumption that D^* represents the radius of a hemisphere centered on the indent, we estimate the volume of the active zone as $V^* = (1/2)[4/3\pi D^{*2}]$. Dividing the energy of indentation, U_i, by this quantity then provides an estimate of the energy density associated with exdent formation in NiTi during an SFM event. Results of this calculation are summarized in Table 4.

Energy densities estimated in this way ranged from 1.2 to 5.3 MJ/m^3. This may be compared to the energy density exerted by an NiTi actuator that undergoes a shape memory strain of 4% under constraint conditions that cause a reaction stress to rise linearly from 0 to 400 MPa during the actuation stroke. This energy is just $U = 1/2\sigma\varepsilon$, or about 8 MJ/m^3. Thus, the formation of exdents in NiTi under the present conditions of constrained recovery appears to carry a very appreciable fraction of the maximum energy density associated with NiTi actuator materials.

4. Conclusion

An indentation-planarization method has been demonstrated for NiTi shape memory alloys that results in two-way shape memory-driven transformation of surface form between flat and bumpy ('exdented') states during thermal cycling. We have termed this phenomenon 'surface form memory,' or SFM. Exdents formed by the SFM effect in NiTi are able to produce replicant indents in a base metal when the latter and the SFM alloy are brought into contact under a suitable preload and then heated.

Consideration of the hardness of the replicant alloy and the depth of the replicant indents leads to the conclusion that SFM involves shape memory energy density greater than 1 MJ/m^3, an appreciable fraction of the theoretical maximum for NiTi SMAs.

The present experiments used single spherical indenters and 'one-shot' shape-memory recovery during exdent formation. Preliminary experiments with cyclically stable exdents indicate that similar indent replication results can be obtained repeatedly from a single NiTi SFM 'tool.' Furthermore, the indentation-planarization technique is even more pronounced when cylindrical indenters are used, and in general, can be readily extended to close-packed indent arrays. In view of the fact that the process operates robustly at the nanoscale, the new technique may be applicable to a wide range of engineering problems from MEMS microassembly to nanolithography to thermally variable friction surfaces.

Acknowledgments

The authors gratefully acknowledge funding from the National Science Foundation under grants CMS0336810 and CMS0510294, and from General Motors Corporation.

References

1. R. Liu, D.Y. Li, Y.S. Xie, R. Llewellyn, and H.M. Hawthorne, Indentation Behavior of Pseudoelastic TiNi Alloy, *Scripta Mater.*, 1999, **41**, p 691
2. F.T. Cheng, P. Shi, and H.C. Man, Correlation of Cavitation Erosion Resistance with Indentation-Derived Properties for a NiTi Alloy, *Scripta Mater.*, 2001, **45**, p 1083
3. K. Gall, K. Juntunen, H.J. Maier, H. Sehitoglu, and Y.I. Chumlyakov, Instrumented Micro-Indentation of NiTi Shape-Memory Alloys, *Acta Mater.*, 2001, **49**, p 3205
4. G.A. Shaw, D.S. Stone, A.D. Johnson, A.B. Ellis, and W.C. Crone, Shape Memory Effect in Nanoindentation of Nickel-Titanium Thin Films, *Appl. Phys. Lett.*, 2003, **83**, p 257
5. X.G. Ma and K. Komvopoulos, Nanoscale Pseudoelastic Behavior of Indented Titanium-Nickel Films, *Appl. Phys. Lett.*, 2003, **83**, p 3773
6. Y.J. Zhang, Y.T. Cheng, and D.S. Grummon, Two-Way Indent Depth Recovery in a NiTi Shape Memory Alloy, *Appl. Phys. Lett.*, 2006, **88**, p 1904
7. Y.J. Zhang, Y.T. Cheng, and D.S. Grummon, Shape Memory Surfaces, *Appl. Phys. Lett.*, 2006, **89**, p 1912
8. D. Tabor, Indentation Hardness: Fifty Years On—A Personal View, *Philos. Mag. A*, 1996, **74**, p 1207
9. D. Tabor, A Simple Theory of Static and Dynamic Hardness, *Proc. R. Soc. Lond. A*, 1948, **192**, p 247
10. X. Fei, Y. Zhang, D.S. Grummon, and Y.-T. Cheng, Indentation-Induced Two-Way Shape Memory Surfaces, *J. Mater. Res.*, Focus issue on Indentation Methods in Advanced Materials Research, in review July, 2008
11. L.E. Samules and T.O. Mulhearn, An Experimental Investigation of the Deformed Zone Associated with Indentation Hardness Impressions, *J. Mech. Phys. Solids*, 1957, **5**, p 125